

COHERENT CURRENT STATES IN MESOSCOPIC FOUR-TERMINAL JOSEPHSON JUNCTION

Malek Zareyan ^a and A.N. Omelyanchouk ^b

^a *Institute for Advanced Studies in Basic Sciences,
45195-159, Gava Zang, Zanjan, Iran*

^b *B.Verkin Institute for Low Temperature Physics and Engineering,
National Academy of Sciences of Ukraine,
47 Lenin Ave., 310164 Kharkov, Ukraine*

December 5, 2017

Abstract

A theory is offered for the ballistic 4-terminal Josephson junction. The studied system consists of a mesoscopic two-dimensional normal rectangular layer which is attached in each side to the bulk superconducting banks (terminals). The relation between the currents through the different terminals, which is valid for arbitrary temperatures and junction sizes, is obtained. The nonlocal coupling of the supercurrents leads to a new effect, specific for the mesoscopic weak link between two superconducting rings; an applied magnetic flux through one of the rings produces a magnetic flux in the other ring even in the absence of an external flux through the other one. The phase dependent distributions of the local density of Andreev states, of the supercurrents and of the induced order parameter are obtained. The "interference pattern" for the anomalous average inside the two dimensional region can be regulated by the applied magnetic fluxes or the transport currents. For some values of the phase differences between the terminals, the current vortex state and the two dimensional phase slip center are appeared.

1 Introduction

The Josephson multiterminal junction presents the microstructure in which the weak coupling takes place between several massive superconducting banks (terminals)[1-3]. Compared with the conventional (2-terminal) Josephson junctions [4] such systems have additional degrees of freedom and corresponding set of the control parameters. With the result, for example, the current- or voltage- biased and the magnetic flux-driven regimes can be combined in one multiterminal junction. The specific multichannel interference effects were studied theoretically and experimentally in the novel superconducting device, the 4-terminal SQUID controlled by the transport current [5-7]. Recently another system based on a Josephson 4-terminal junction was studied [8]. It consists of two superconducting rings, each interrupted by a Josephson junction, which are at the same time weakly coupled with each other. The macroscopic quantum states of such composite system can be regulated by the difference of the magnetic fluxes applied through the rings, in analogy with the phase difference between two weakly coupled bulk superconductors. The nonlinear coupling via the Josephson 4-terminal leads to the cooperative behaviour of the rings in some region of the applied magnetic fluxes, which was called [8] magnetic flux locking.

The 4-terminal junction, which was studied in Refs. [5-8], is a system of short microbridges going from a weak point to massive superconducting banks (Fig.1a). The order parameter (both its amplitude and phase) in the common centre is a function of the currents through all the microbridges. The supercurrent flowing into the i th bank is determined by the phases of the order parameter φ_i , ($i = 1, ..4$) in all the banks [5]:

$$I_i = \frac{\pi\Delta_0^2(T)}{4eT_c} \frac{1}{\sum_j 1/R_j} \sum_j \frac{1}{R_i R_j} \sin(\varphi_i - \varphi_j). \quad (1)$$

The relation (1) was obtained in the frame of the Ginzburg-Landau approach, which is valid for temperatures T close to the critical temperature T_c . As it was pointed in the Ref. [8], the macroscopic interference effects due to coupling of supercurrents in different terminals are not restricted by the special kind of the 4-terminal junction (Fig.1a). In fact, any mesoscopic 4-terminal weak link will produce a coupling similar to the relation (1). In the present paper, the microscopic theory of the mesoscopic ballistic 4-terminal

junction is developed. We consider a Josephson weak coupling through the two-dimensional normal layer which is connected with four bulk superconducting terminals as it is shown in Fig.1b. Such a S-2DEG-S structure was experimentally realized in Ref. [9] for the case of two terminals. It was shown in [9] that this new class of fully phase coherent Josephson junctions demonstrate the nonlocal phase dependence of mesoscopic supercurrents. We study the coherent current states in such a 4-terminal structure within the quasiclassical equations for transport-like Green's functions. The relation between the currents in the different terminals, which is valid for arbitrary temperatures and junction sizes, is obtained. The structure of current carrying states inside the mesoscopic 4-terminal junction presents the interest itself. As it is well known (see e.g. [10]), in ballistic Josephson junction with direct conductivity the supercurrent flows through the local Andreev levels. In multiterminal case considered here, the spatial distribution of current density and of the order parameter, and hence the phase-dependent Andreev levels, are determined by the phase differences between all terminals. Thus, they can be regulated by the external control parameters, i.e. the transport currents and (or) the applied magnetic fluxes. In Section 2, we present the description of the system and formulate basic equations and boundary conditions. In Section 3 the current-phase relations analogous to (1) are derived for the cases of small (as compared to the coherence length) and also arbitrary junction sizes. The spatial distributions of the supercurrent density and of the induced order parameter are studied in Section 4.

2 Model and basic equations.

The studied system consists of 4 bulk superconducting banks which are contacted with 4 sides of rectangular two-dimensional (2D) normal layer having the length L and width W (see Figs. 1b and 2). The sizes L and W are supposed to be much larger than Fermi wave-length $\lambda_F = h/p_F$. To study the stationary coherent current states in 4-terminal ballistic junction we use the Eilenberger equations [11] for ξ -integrated Green's functions:

$$\mathbf{v}_F \frac{\partial}{\partial \mathbf{r}} \hat{G} + [\omega \hat{\tau}_3 + \hat{\Delta}, \hat{G}] = 0, \quad (2)$$

where

$$\hat{G}_\omega(\mathbf{v}_F, \mathbf{r}) = \begin{pmatrix} g_\omega & f_\omega \\ f_\omega^+ & -g_\omega \end{pmatrix}$$

is the matrix Green's function, which depends on the Matsubara frequency ω , the electron velocity on the Fermi surface \mathbf{v}_F and the coordinate \mathbf{r} ;

$$\hat{\Delta} = \begin{pmatrix} 0 & \Delta \\ \Delta^* & 0 \end{pmatrix}$$

is the superconducting pair potential. For the self-consistent off-diagonal potential $\Delta(\mathbf{r})$ and current density $\mathbf{j}(\mathbf{r})$ we have the expressions

$$\Delta(\mathbf{r}) = \lambda 2\pi T \sum_{\omega>0} \langle f_\omega \rangle, \quad (3)$$

$$\mathbf{j}(\mathbf{r}) = -4\pi i e N(0) T \sum_{\omega>0} \langle \mathbf{v}_F g_\omega \rangle. \quad (4)$$

They determine the induced order parameter $\Psi \equiv \Delta/\lambda$ and the 2D current density in the normal layer; $N(0) = \frac{m}{2\pi}$, $\langle \dots \rangle$ is the averaging over directions of 2D vector \mathbf{v}_F , λ is the constant of electron-phonon coupling.

The equations (2) are supplemented by the values of Δ and Green's functions in bulk banks far from the S-N interfaces:

$$\hat{\Delta}_i = \Delta_0(\hat{\tau}_1 \cos \varphi_i - \hat{\tau}_2 \sin \varphi_i), \quad \hat{G}_i = \frac{\omega \hat{\tau}_3 + \hat{\Delta}_i}{\sqrt{\omega^2 + \Delta_0^2}}, \quad i = 1, \dots, 4. \quad (5)$$

We solve Eqs. (2) by integrating over the "transit" trajectories of the ballistic flight of electrons from one bank to another [12]. These trajectories (characteristics of the differential Eqs.(2)) are straight lines along the direction of electron velocity (see Fig. 2). In the bulk superconducting banks the order parameter can be taken as the constant value (5) up to the S-N interface. In contrast to the case of 2D banks these "rigid" conditions for Δ [1, 12] are valid for arbitrary sizes L and W compared with the coherence length $\xi_0 \sim v_F/\Delta_0$, and not only for $L, W \gg \xi_0$. At the same time, the Green's function along the given transit trajectory varies in a distance of about ξ_0 where approaching the S-N interface.

Let us introduce the time of flight along the trajectory, $\mathbf{v}_F \frac{\partial}{\partial \mathbf{r}} \equiv \frac{d}{dt}$, $t_i < t < \infty$ where $t = t_i$ corresponds to the point on i th S-N boundary and $t = \infty$ to the point inside i th bank far from the S-N boundary. Then the general solution of Eqs.(2) inside the i th bank satisfying the boundary conditions (5) will be

$$\begin{aligned} \hat{G}_i(t) &= \frac{\omega \hat{\tau}_3 + \hat{\Delta}_i}{\Omega} \\ &+ C_i [\Delta_0 \hat{\tau}_3 - (\omega \cos \varphi_i + i \text{sign}(\mathbf{v}_F \mathbf{n}_i) \Omega \sin \varphi_i) \hat{\tau}_1 \\ &+ (\omega \sin \varphi_i - i \text{sign}(\mathbf{v}_F \mathbf{n}_i) \Omega \cos \varphi_i) \hat{\tau}_2] e^{-2\Omega(t-t_i)}. \end{aligned} \quad (6)$$

Here \mathbf{n}_i is the outer normal to the i th side of the rectangular boundary and $\Omega = \sqrt{\omega^2 + \Delta_0^2}$. The arbitrary constants C_i must be found by matching of Green's functions at in-coming and out-going points at S-N boundaries with the solution inside the normal layer along the trajectory which connects these points (see Fig. 2). We consider here the simplest case when only Andreev reflection [13] occurs at S-N interface. In more realistic case, when usual reflection (e.g. due to the potential barrier) or interface roughness are present, more general matching conditions must be used (see [14]).

3 Current-Phase relations

Inside the normal layer ($\Delta = 0$), the Eilenberger equations can be solved analytically. If we classify the electronic trajectories inside the normal layer according to the sides at which they come in and go out, then the solution of eq. (2) can be written as

$$\begin{aligned} \hat{G}_{i \rightarrow j}(t) &= \frac{\omega}{\Omega} \hat{\tau}_3 + \frac{\Delta_0}{\Omega} \{ \cosh [2\omega(t - t_i) - i\varphi_i] \hat{\tau}_1 - i \sinh [2\omega(t - t_i) - i\varphi_i] \hat{\tau}_2 \} \\ &+ A_{i \rightarrow j} \{ \Delta_0 \hat{\tau}_3 - [\omega \cosh (2\omega(t - t_i) - i\varphi_i) + \Omega \sinh (2\omega(t - t_i) - i\varphi_i)] \hat{\tau}_1 \\ &+ i [\Omega \cosh (2\omega(t - t_i) - i\varphi_i) + \omega \sinh (2\omega(t - t_i) - i\varphi_i)] \hat{\tau}_2 \}, \end{aligned} \quad (7)$$

where $\hat{G}_{i \rightarrow j}(t)$ is the matrix Green's function along the trajectory originating in the i th side and extending to the j th side (see Fig. 2). We denote

this trajectory by $i \rightarrow j$. Matching (7) with solution in the banks (6), the corresponding $A_{i \rightarrow j}$ is obtained

$$A_{i \rightarrow j} = \frac{\frac{\Delta_0}{\Omega} \sinh(\omega t_{ji} + i \frac{\varphi_{ji}}{2})}{\omega \sinh(\omega t_{ji} + i \frac{\varphi_{ji}}{2}) + \Omega \cosh(\omega t_{ji} + i \frac{\varphi_{ji}}{2})}, \quad (8)$$

where $t_{ji} = t_j - t_i$ and $\varphi_{ji} = \varphi_j - \varphi_i$. From (7) and (8) we have the expression for matrix Green's function $\hat{G}_\omega(\vec{\rho}, \mathbf{v}_F)$ as a function of the coordinate $\vec{\rho} \in \Sigma$ (Σ is the region of 2D rectangular weak link) and the direction of \mathbf{v}_F . In fact we can write

$$\hat{G}_\omega(\vec{\rho}, \mathbf{v}_F) = \hat{G}_{i \rightarrow j}, \quad \text{for } \mathbf{v}_F \in \theta_{ij}(\vec{\rho}), \quad (9)$$

where we have introduced $\theta_{ij}(\vec{\rho})$ as the angle in which all $i \rightarrow j$ trajectories, passing through the point $\vec{\rho}$, are confined (see Fig. 2, eq. (A1) in Appendix). The diagonal and off-diagonal terms of $\hat{G}_{i \rightarrow j}$ have the forms

$$\begin{aligned} g_{i \rightarrow j} &= \frac{\omega}{\Omega} + \Delta_0 A_{i \rightarrow j} \\ &= \frac{\omega \cosh(\omega t_{ji} + i \frac{\varphi_{ji}}{2}) + \Omega \sinh(\omega t_{ji} + i \frac{\varphi_{ji}}{2})}{\Omega \cosh(\omega t_{ji} + i \frac{\varphi_{ji}}{2}) + \omega \sinh(\omega t_{ji} + i \frac{\varphi_{ji}}{2})}, \end{aligned} \quad (10)$$

$$\begin{aligned} f_{i \rightarrow j} &= \left[\frac{\Delta_0}{\Omega} + (\Omega - \omega) A_{i \rightarrow j} \right] \exp[-2\omega(t - t_i) + i\varphi_i] \\ &= \frac{\Delta_0 \exp(\omega t_{ji} + i \frac{\varphi_i + \varphi_j}{2})}{\Omega \cosh(\omega t_{ji} + i \frac{\varphi_{ji}}{2}) + \omega \sinh(\omega t_{ji} + i \frac{\varphi_{ji}}{2})} e^{-2\omega(t - t_i)}. \end{aligned} \quad (11)$$

In the limit $L, W \ll \xi_0$ the expressions (10) and (11) for Green's functions are simplified and we have

$$g_{i \rightarrow j} = \frac{\omega \Omega + i \frac{1}{2} \Delta_0^2 \sin(\varphi_{ji})}{\omega^2 + \Delta_0^2 \cos^2(\frac{\varphi_{ji}}{2})}, \quad (12)$$

$$f_{i \rightarrow j} = \frac{\Delta_0}{\Omega \cos(\frac{\varphi_{ji}}{2}) + i\omega \sin(\frac{\varphi_{ji}}{2})} \exp\left(\frac{\varphi_i + \varphi_j}{2}\right). \quad (13)$$

We can obtain the retarded and advanced Green's functions, $\hat{G}^{R,A}(\epsilon)$, by analytical continuation of Matsubara Green's function $\hat{G}(\omega)$ (eqs. (9)-(13)). The poles of diagonal component of the retarded Green's function,

$g^R(\epsilon, \vec{\rho}, \mathbf{v}_F)$, determine the energies of local Andreev states in the system. The local density of states in the normal layer is given by the formula

$$\mathcal{N}(\epsilon, \vec{\rho}) = N(0) \langle \text{Re } g(\omega = -i\epsilon, \vec{\rho}, \mathbf{v}_F) \rangle. \quad (14)$$

Using the expressions (9), (12) and the fact that, $\theta_{ij}(\vec{\rho}) = \theta_{ji}(\vec{\rho})$, in the case of small junction, we obtain:

$$\begin{aligned} \mathcal{N}(\epsilon, \vec{\rho}, \{\varphi_i\}) &= N(0) \sum_{i \neq j} \langle \text{Re } g(\omega = -i\epsilon, \vec{\rho}, \mathbf{v}_F) \rangle_{\theta_{ij}} \\ &= N(0) \sum_{i \neq j} \theta_{ij}(\vec{\rho}) \text{Re } g_{i \rightarrow j}(\omega = -i\epsilon) \\ &= N(0) \sum_{i < j} \theta_{ij}(\vec{\rho}) \text{Re} [g_{i \rightarrow j}(\omega = -i\epsilon) + g_{j \rightarrow i}(\omega = -i\epsilon)] \\ &= \pi \Delta_0 N(0) \sum_{i < j} \theta_{ij}(\vec{\rho}) \left| \sin \frac{\varphi_{ji}}{2} \right| \delta(|\epsilon| - \Delta_0 \cos \frac{\varphi_{ji}}{2}). \end{aligned} \quad (15)$$

We can also use eqs. (9) and (12) to obtain $\langle \mathbf{v}_F g \rangle$ at a point of the i th side $\vec{\rho}_i$. Then, the resulting expression can be replaced in eq. (4) to find the current density $\mathbf{j}(\vec{\rho}_i)$. The calculation of the current density at the arbitrary point of the normal rectangular will come in the next section and the appendix. Here we calculate the total current I_i flowing into the i th bank.

Let us start with the case of a small junction ($L, W \ll \xi_0$). In order to find I_i , we have to calculate the integral $I_i = \int_{(S_i)} \mathbf{j}(\vec{\rho}_i) \cdot \mathbf{ds}_i$, where the integral is taken over the i th side of rectangular.

After calculation of $\mathbf{j}(\vec{\rho}_i)$ from (A3) and (A5) and taking the integral over \mathbf{ds}_i , we obtain for the current I_i

$$I_i = \frac{e p_F \Delta_0 d}{2\pi} \sum_{j=1}^4 \gamma_{ij} \sin \left(\frac{\varphi_i - \varphi_j}{2} \right) \tanh \left[\frac{\Delta_0 \cos \left(\frac{\varphi_i - \varphi_j}{2} \right)}{2T} \right] \quad (16)$$

where $d = \sqrt{L^2 + W^2}$ and $\gamma_{ij} = \gamma_{ji}$,

$$\begin{aligned} \gamma_{13} &= 1 - \frac{k}{\sqrt{1+k^2}}, \\ \gamma_{24} &= 1 - \frac{1}{\sqrt{1+k^2}}, \end{aligned}$$

$$\gamma_{12} = \gamma_{14} = \gamma_{23} = \gamma_{34} = \frac{1}{2} \left(\frac{1+k}{\sqrt{1+k^2}} - 1 \right), \quad (17)$$

are geometrical form factors which depend on the width to length ratio $k = W/L$. The positive sign of I_i corresponds to the direction of the current from the normal layer to the i th bank. Note that $\sum_{i=1}^4 I_i = 0$.

The formula (16) for current-phase relations generalizes the expression (1) to the case of a small mesoscopic 4-terminal junction. It follows from (17) that the form factor γ_{ij} can not be factorized, i.e., presented in the form $\gamma_{ij} = \gamma_i \gamma_j$, in contrast to the case of relation (1) where $\gamma_{ij} = \frac{1}{R_i} \cdot \frac{1}{R_j}$. This essential feature of the current-phase relations reflects the nonlocal nature of the supercurrents in the mesoscopic multi-terminal Josephson junction.

The current-phase relations (16) are valid for arbitrary temperature T . In the limiting cases of $T = 0$ and temperature close to T_c the expression (16) takes the forms

$$I_i = \frac{ep_F \Delta_0 d}{2} \sum_{j=1}^4 \gamma_{ij} \sin \left(\frac{\varphi_i - \varphi_j}{2} \right) \quad \text{for } T = 0, \quad (18)$$

$$I_i = \frac{ep_F \Delta_0^2 d}{4\pi T_c} \sum_{j=1}^4 \gamma_{ij} \sin (\varphi_i - \varphi_j) \quad \text{for } T \simeq T_c. \quad (19)$$

In the case of arbitrary lengths L, W we restrict the consideration for the temperature close to T_c . In this case the current-phase relations similar to the expression (19) can be obtained. The difference is in geometrical form factors. In fact we have the result

$$I_i = \frac{ep_F \Delta_0^2 d}{4\pi T_c} \sum_{j=1}^4 \tilde{\gamma}_{ij}(k, L, W) \sin (\varphi_i - \varphi_j) \quad (20)$$

where the generalized form factors are given by

$$\begin{aligned} \tilde{\gamma}_{41} = \tilde{\gamma}_{21} = \tilde{\gamma}_{23} = \tilde{\gamma}_{43} = \\ \frac{4}{\pi^2 \sqrt{1+k^2}} \int_{-\frac{k}{2}}^{\frac{k}{2}} dy \int_{\arctan(\frac{k}{2}+y)}^{\frac{\pi}{2}} d\theta \cos \theta \sum_{n=0}^{\infty} \frac{\exp \left[-\frac{L(\frac{k}{2}+y)}{\xi_N \cos \theta} (2n+1) \right]}{(2n+1)^2}, \end{aligned}$$

$$\tilde{\gamma}_{42} = \tilde{\gamma}_{24} = \frac{4}{\pi^2 \sqrt{1+k^2}} \int_{-\frac{k}{2}}^{\frac{k}{2}} dy \int_{-\arctan(\frac{k}{2}+y)}^{\arctan(\frac{k}{2}-y)} d\theta \cos \theta \sum_{n=0}^{\infty} \frac{\exp[-\frac{L}{\xi_N \cos \theta} (2n+1)]}{(2n+1)^2}, \quad (21)$$

$$\tilde{\gamma}_{12} = \tilde{\gamma}_{14} = \tilde{\gamma}_{32} = \tilde{\gamma}_{34} = \tilde{\gamma}_{41} (L \rightarrow W, W \rightarrow L, k \rightarrow \frac{1}{k}),$$

$$\tilde{\gamma}_{13} = \tilde{\gamma}_{31} = \tilde{\gamma}_{42} (L \rightarrow W, W \rightarrow L, k \rightarrow \frac{1}{k}).$$

Here $\xi_N = \frac{v_F}{2\pi T}$. In the limit $L, W \ll \xi_0$, $\tilde{\gamma}_{ij}$ reduce to γ_{ij} .

4 Spatial distribution of supercurrents and induced order parameter

In this section we will obtain the supercurrent density and the induced order parameter at an arbitrary point of the normal layer in the case of small junction. At the given point of the normal layer $\vec{\rho} = x\mathbf{i} + y\mathbf{j}$

$$\begin{aligned} \langle \mathbf{v}_{\mathbf{F}} g \rangle &= \sum_{i>j} (\langle \mathbf{v}_{\mathbf{F}} g \rangle_{\theta_{ij}} + \langle \mathbf{v}_{\mathbf{F}} g \rangle_{\theta_{ji}}) \\ &= i \sum_{i>j} \langle \mathbf{v}_{\mathbf{F}} \rangle_{\theta_{ij}} \frac{\Delta_0^2 \sin \varphi_{ji}}{\omega^2 + \Delta_0^2 \cos^2 \frac{\varphi_{ji}}{2}} \end{aligned} \quad (22)$$

where we have used $\langle \mathbf{v}_{\mathbf{F}} g \rangle_{\theta_{ij}} = \langle \mathbf{v}_{\mathbf{F}} \rangle_{\theta_{ij}} g_{i \rightarrow j}$, $\langle \mathbf{v}_{\mathbf{F}} \rangle_{\theta_{ji}} = -\langle \mathbf{v}_{\mathbf{F}} \rangle_{\theta_{ij}}$ and $g_{j \rightarrow i} = g_{i \rightarrow j}^*$.

Replacing (22) in the eq. (4) the current density is obtained

$$\mathbf{j}(\vec{\rho}) = 2\pi e N(0) \Delta_0 \sum_{i>j} \langle \mathbf{v}_{\mathbf{F}} \rangle_{\theta_{ij}} \sin \frac{\varphi_{ji}}{2} \tanh \left(\frac{\Delta_0 \cos \frac{\varphi_{ji}}{2}}{2T} \right) \quad (23)$$

The expression (23) describes the spatial distribution of the current density inside the normal layer. In order to find the explicit expression for the coefficients $\langle \mathbf{v}_{\mathbf{F}} \rangle_{\theta_{ij}}$ in eq. (23), we have to consider 4 different regions in the normal rectangular and obtain $\mathbf{j}(\vec{\rho})$ in each region separately (see Appendix). This calculation has been done in the appendix and the result for $\mathbf{j}(\vec{\rho})$ is given by (A3) and (A5). Here we write eq. (23) in the more transparent form. Let

us introduce $\hat{\theta}_{ij}(\vec{\rho})$ as the unit vector in the direction of the $i \rightarrow j$ trajectory passing through the bisector of $\theta_{ij}(\vec{\rho})$; then, $\langle \mathbf{v}_F \rangle_{\theta_{ij}}$ can be written as

$$\langle \mathbf{v}_F \rangle_{\theta_{ij}} = \int_0^{\theta_{ij}} \frac{d\theta}{2\pi} \mathbf{v}_F = \frac{v_F}{\pi} \sin\left(\frac{\theta_{ij}}{2}\right) \hat{\theta}_{ij}. \quad (24)$$

Combining eqs. (23) and (24), we obtain

$$\mathbf{j}(\vec{\rho}) = \frac{ep_F \Delta_0}{2\pi} \sum_{i < j} \sin\left(\frac{\theta_{ij}}{2}\right) \hat{\theta}_{ij}(\vec{\rho}) \sin\left(\frac{\varphi_j - \varphi_i}{2}\right) \tanh\left[\frac{\Delta_0 \cos\left(\frac{\varphi_j - \varphi_i}{2}\right)}{2T}\right]. \quad (25)$$

In the way similar to what we have done for $\mathbf{j}(\vec{\rho})$, the distribution of the induced order parameter can be obtained. In this case we need to calculate the average of off-diagonal element of the matrix Green's function, $f_\omega(\mathbf{v}_F, \vec{\rho})$, on the direction of \mathbf{v}_F :

$$\langle f \rangle = \sum_{i \neq j} \langle f \rangle_{\theta_{ij}} = \sum_{i \neq j} \theta_{ij}(\vec{\rho}) f_{i \rightarrow j}. \quad (26)$$

Replacing (26) in (3) and after the calculation, we obtain for $\Psi(x, y) = \Delta(x, y)/\lambda$:

$$\Psi(x, y) = \frac{\Delta_0}{\lambda} \sum_{i=1}^4 \theta_i(x, y) e^{i\varphi_i}. \quad (27)$$

Here $\theta_i(x, y)$ is the angle by which i th side is seen from the point $\vec{\rho} \equiv (x, y)$. The angles $\theta_i(x, y)$'s are given by the relations

$$\begin{aligned} \theta_1 &= \pi - \alpha(x, y) - \alpha(-x, y), & \theta_2 &= \alpha(-x, -y) + \alpha(-x, y), \\ \theta_3 &= \pi - \alpha(x, -y) - \alpha(-x, -y), & \theta_4 &= \alpha(x, y) + \alpha(x, -y). \end{aligned} \quad (28)$$

where the angle

$$\alpha(x, y) = \arctan\left(\frac{k/2 + y}{1/2 + x}\right), \quad (29)$$

is a function of the coordinate (normalized by L) and is shown in Fig. 6. Eq.(27) expresses the fact that, inside the ballistic normal layer region the linear superposition of four macroscopic wave functions (pair potentials) of the banks occurs, where the weight of wave function of the i th bank is determined by the geometrical factor $\theta_i(x, y)$.

5 Conclusions

The present study considers a 4-terminal microstructure based on a new class of mesoscopic Josephson junctions [9] which are fully phase coherent and have comparable width and length. The microscopic theory of the stationary coherent current states in ballistic multiterminals is developed.

We have calculated the current-phase relations (CPR), i.e. the total currents in each terminal as functions of the phases of the superconducting order parameter in all the banks. These relations describe the behaviour of the system influenced by the external transport currents or the applied magnetic fluxes. The essential difference between the CPR for mesoscopic (expression (19)) and conventional (relation (1)) 4-terminals consists in the structure of the coefficients of coupling γ_{ij} . In the mesoscopic case considered here these coefficients can not be factorized (presented in the form $\gamma_{ij} = \gamma_i \gamma_j$) for all indexes i, j and arbitrary value of the width to length ratio $k = W/L$. Here we only outline the new effect, specific for the mesoscopic 4-terminal junction, which follows from such nonlocal coupling of the currents. Let us consider the configuration shown in Fig. 3. By using the CPR (19) with γ_{ij} given by (17), it can be shown that an applied magnetic flux through one of the rings produces magnetic flux in the other ring even in the absence of an external flux through the other one. The detailed theory of this effect will be reported in a separate publication.

The physical properties of the interior of the mesoscopic 4-terminal junction present the interest themselves. The above calculated local density of Andreev states, the current density and the order parameter distributions depend on the phase differences between the four terminals and can be regulated by the applied magnetic fluxes. In particular, for some values of the phases φ , θ and χ (see Fig. 3) the "vortex state" inside the mesoscopic 2D weak link exists. Figures 4 and 5 present the plots for distributions of the absolute value of the induced order parameter and the supercurrent density in the case $\theta = \pi/2$, $\varphi = 3\pi/2$, $\chi = 0$. The studying of the structure of induced order parameter and local density of states, as well as the dynamical behaviour of the system will be the object of further investigation.

Acknowledgments

The authors would like to acknowledge support for this research from the Institute for Advanced Studies in Basic Sciences at Zanjan, IRAN. We

acknowledge to R.de Bruyn Ouboter and I.O.Kulik for usefull discussions.

Appendix

In this appendix we present expressions for the angles θ_{ij} and the vectors $\langle \mathbf{v}_F \rangle_{\theta_{ij}}$. Using the expressions given here, one can calculate the density of states \mathcal{N} and the current density \mathbf{j} [see eqs. (15) and (23)].

According to the classification of the trajectories in term of origin and destination sides, there are 12 different types of trajectories which are $1 \rightarrow 2, 1 \rightarrow 3, 1 \rightarrow 4, 2 \rightarrow 3, 2 \rightarrow 4, 3 \rightarrow 4$ and the corresponding reverse of these trajectories. For a given point, depending on the position, some of these trajectories do not take place. In this respect we can consider four different regions in the normal rectangular: *I* where $y < 0, |y| > k|x|$, ($2 \rightarrow 3, 3 \rightarrow 4$ and their reversed are absent)

II where $x \geq 0, |y| \leq kx$, ($1 \rightarrow 4, 3 \rightarrow 4$ and their reversed are absent),

III where $y \geq 0, y > k|x|$, ($1 \rightarrow 2, 1 \rightarrow 4$ and their reversed are absent) and

IV where $x < 0, |y| \leq kx$, ($1 \rightarrow 2, 2 \rightarrow 3$ and their reversed are absent).

At the given point $\vec{\rho}$, for the absent trajectories we have $\theta_{ij} = 0$, and consequently the corresponding term in the expressions of \mathcal{N} and \mathbf{j} [eqs. (15) and (23)] will vanish. We will calculate \mathbf{j} in the given point of the region *II* and then introduce the exchange rules of arguments to obtain it in other regions. Consider a point in region *II*; the possible (non-vanishing) θ_{ij} are drawn in Fig. 6 and, can be expressed in terms θ_i 's (given by (28) and(29)) as

$$\begin{aligned}\theta_{12} &= \frac{1}{2}(\theta_1 + \theta_2 - \theta_3 - \theta_4) \\ \theta_{13} &= \frac{1}{2}(\theta_1 - \theta_2 + \theta_3 + \theta_4) \\ \theta_{23} &= \frac{1}{2}(-\theta_1 + \theta_2 + \theta_3 - \theta_4) \\ \theta_{24} &= \theta_4\end{aligned}\tag{A1}$$

Also we can use the relation, $\langle \mathbf{v}_F \rangle_{\theta_{ij}} = \int_{(\theta_{ij})} \frac{d\theta}{2\pi} v_F (\cos \theta \mathbf{i} + \sin \theta \mathbf{j})$, to obtain

$$\begin{aligned}\langle \mathbf{v}_F \rangle_{\theta_{12}}(x, y) &= \frac{v_F}{2\pi} \{ [\sin[\alpha(-x, -y)] - \sin[\alpha(x, y)]] \mathbf{i} \\ &+ [\cos[\alpha(x, y)] - \cos[\alpha(-x, -y)]] \mathbf{j} \}\end{aligned}$$

$$\begin{aligned}
\langle \mathbf{v}_F \rangle_{\theta_{13}}(x, y) &= \frac{v_F}{2\pi} \{ [\sin[\alpha(-x, y)] - \sin[\alpha(-x, -y)]] \mathbf{i} \\
&\quad + [\cos[\alpha(-x, y)] + \cos[\alpha(-x, -y)]] \mathbf{j} \} \\
\langle \mathbf{v}_F \rangle_{\theta_{23}}(x, y) &= \frac{v_F}{2\pi} \{ [\sin[\alpha(x, -y)] - \sin[\alpha(-x, y)]] \mathbf{i} \\
&\quad + [\cos[\alpha(x, -y)] - \cos[\alpha(-x, y)]] \mathbf{j} \} \\
\langle \mathbf{v}_F \rangle_{\theta_{24}}(x, y) &= \frac{v_F}{2\pi} \{ -[\sin[\alpha(x, y)] + \sin[\alpha(x, -y)]] \mathbf{i} \\
&\quad + [\cos[\alpha(x, y)] - \cos[\alpha(x, -y)]] \mathbf{j} \} \tag{A2}
\end{aligned}$$

with $\alpha(x, y)$ is given by eq. (29). The corresponding relations valid for other regions, can be obtained from (A1) and (A2), using the appropriate rules of index and coordinate exchanging (see below).

Replacing eqs. (A1) and (A2) in (23), we obtain for current density in a point of region II , \mathbf{j}_{II}

$$\begin{aligned}
\mathbf{j}_{II}(x, y) &= [-\mathbf{k}(x, y) + \mathbf{l}(x, y)]P_{13} + [\mathbf{k}(-x, -y) - \mathbf{k}(x, y)]P_{12} \\
&\quad - [\mathbf{k}(x, y) + \mathbf{l}(-x, -y)]P_{24} + [\mathbf{l}(-x, -y) - \mathbf{l}(x, y)]P_{23}, \tag{A3}
\end{aligned}$$

where

$$\begin{aligned}
\mathbf{k}(x, y) &= \sin \alpha(x, y) \mathbf{i} - \cos \alpha(x, y) \mathbf{j}, \\
\mathbf{l}(x, y) &= \sin \alpha(-x, y) \mathbf{i} + \cos \alpha(-x, y) \mathbf{j}, \tag{A4}
\end{aligned}$$

and $P_{ij} = \frac{ep_F \Delta_0}{2\pi} \sin \frac{\varphi_{ji}}{2} \tanh \left(\frac{\Delta_0 \cos \frac{\varphi_{ji}}{2}}{2T} \right)$. The current density in other regions is obtained from \mathbf{j}_{II} by applying the following rules of phase and coordinate exchanging

$$\begin{aligned}
\mathbf{j}_I &= \mathbf{j}_{II}[(x \rightarrow -y/k, y \rightarrow x/k, k \rightarrow 1/k); (\mathbf{i} \rightarrow -\mathbf{j}, \mathbf{j} \rightarrow \mathbf{i}); \\
&\quad (\varphi_1 \rightarrow \varphi_4, \varphi_2 \rightarrow \varphi_1, \varphi_3 \rightarrow \varphi_2, \varphi_4 \rightarrow \varphi_3)], \\
\mathbf{j}_{III} &= \mathbf{j}_{II}[(x \rightarrow y/k, y \rightarrow -x/k, k \rightarrow 1/k); (\mathbf{i} \rightarrow \mathbf{j}, \mathbf{j} \rightarrow -\mathbf{i}); \\
&\quad (\varphi_1 \rightarrow \varphi_2, \varphi_2 \rightarrow \varphi_3, \varphi_3 \rightarrow \varphi_4, \varphi_4 \rightarrow \varphi_1)], \tag{A5} \\
\mathbf{j}_{IV} &= \mathbf{j}_{II}[(x \rightarrow -x, y \rightarrow -y, k \rightarrow k); (\mathbf{i} \rightarrow -\mathbf{i}, \mathbf{j} \rightarrow -\mathbf{j}); \\
&\quad (\varphi_1 \rightarrow \varphi_3, \varphi_2 \rightarrow \varphi_4, \varphi_3 \rightarrow \varphi_1, \varphi_4 \rightarrow \varphi_2)].
\end{aligned}$$

The same relations as (A5) can be used for θ_{ij} and $\langle \mathbf{v}_F \rangle_{\theta_{ij}}$ (the phase exchanges have to be replaced by corresponding index exchanges).

References

- [1] K. K. Likharev, Rev. Mod. Phys. 51 (1979).
- [2] I.O.Kulik, A.N.Omelyanchouk, E. A. Kel'man, Sov.J. Low Temp. Phys. 5 (1979) 55.
- [3] E. D. Vol, A.N.Omelyanchouk, Low Temp. Phys. 20 (1994) 87.
- [4] A. Barone and G. Paterno, Physics and applications of the Josephson effect, Wiley, New York, 1982.
- [5] R. de Bruyn Ouboter, A.N.Omelyanchouk, E. D. Vol, Physica B 205 (1995) 153; 239 (1997) 203.
- [6] B. J. Vleeming, A. V. Zakarian, A.N.Omelyanchouk, R. de Bruyn Ouboter, Physica B 226 (1996) 253; Czechoslovak Journal of Physics 46,S5 2823 (1996).
- [7] B. J. Vleeming, PhD thesis, Leiden University (1998).
- [8] R. de Bruyn Ouboter, A.N.Omelyanchouk, E. D. Vol, to be published in Low Temp. Phys. 24, N10 (1998); Los Alamos archive cond-mat/9805174.
- [9] J. P. Heida, B. J. van Wees, T. M. Klapwijk and G. Borghs, Phys. Rev. B 57, R5618 (1998).
- [10] P. F. Bagwell, R. Riedel, L. Chang, Physica B 203 (1994) 475.
- [11] G. Eilenberger, Zs. Phys., 214, 195 (1968).
- [12] I.O.Kulik and A.N.Omelyanchouk, Sov.J. Low Temp. Phys. 4, 142 (1978).
- [13] A. F. Andreev, Sov. Phys. JETP 19, 1228 (1964).
- [14] A.N.Omelyanchouk, R. de Bruyn Ouboter and C. J. Muler, Low Temp. Phys. 20, 398 (1994).

Figure Captions

Figure 1. (a) The superconducting 4-terminal Josephson junction. Four coupled superconducting microbridges, going from a weak point to the massive superconducting banks (R_i is the normal resistance of the i th filament and $\xi(T)$ is the coherence length).

(b) The mesoscopic 4-terminal Josephson junction. Four bulk superconductors are weakly coupled through a rectangular of two-dimensional electron gas (2DEG).

Figure 2. Dashed line is $i \rightarrow j$ trajectory passing through the point $\vec{\rho}$. All of this type trajectories are confined in the angle θ_{ij} . L , W are length and width of the rectangular.

Figure 3. A configuration of the mesoscopic 4-terminal Josephson junction. The terminals 1 with 2, and 3 with 4 are short-circuited by the superconducting rings (dashed lines). The phase differences are $\theta = \varphi_2 - \varphi_1$, $\varphi = \varphi_3 - \varphi_4$, $\chi = \frac{\varphi_1 + \varphi_2}{2} - \frac{\varphi_3 + \varphi_4}{2}$.

Figure 4. Absolute value of the induced order parameter $|\psi(x, y)|$ is plotted vertically for the values of phase differences $\theta = \varphi_2 - \varphi_1 = \pi/2$, $\varphi = \varphi_3 - \varphi_4 = 3\pi/2$, $\chi = \frac{\varphi_1 + \varphi_2}{2} - \frac{\varphi_3 + \varphi_4}{2} = 0$. The lines of $|\psi(x, y)| = \text{const.}$ are shown.

Figure 5. Vector field plot of the supercurrent density, $\mathbf{j}(x, y)$, inside the normal layer. The values of phase differences are the same as the Fig. 4.

Figure 6. The angles θ_{ij} for a point in the region II . We have just shown θ_{13} , θ_{23} , $\theta_{24} = \theta_4$ and also the angle α .

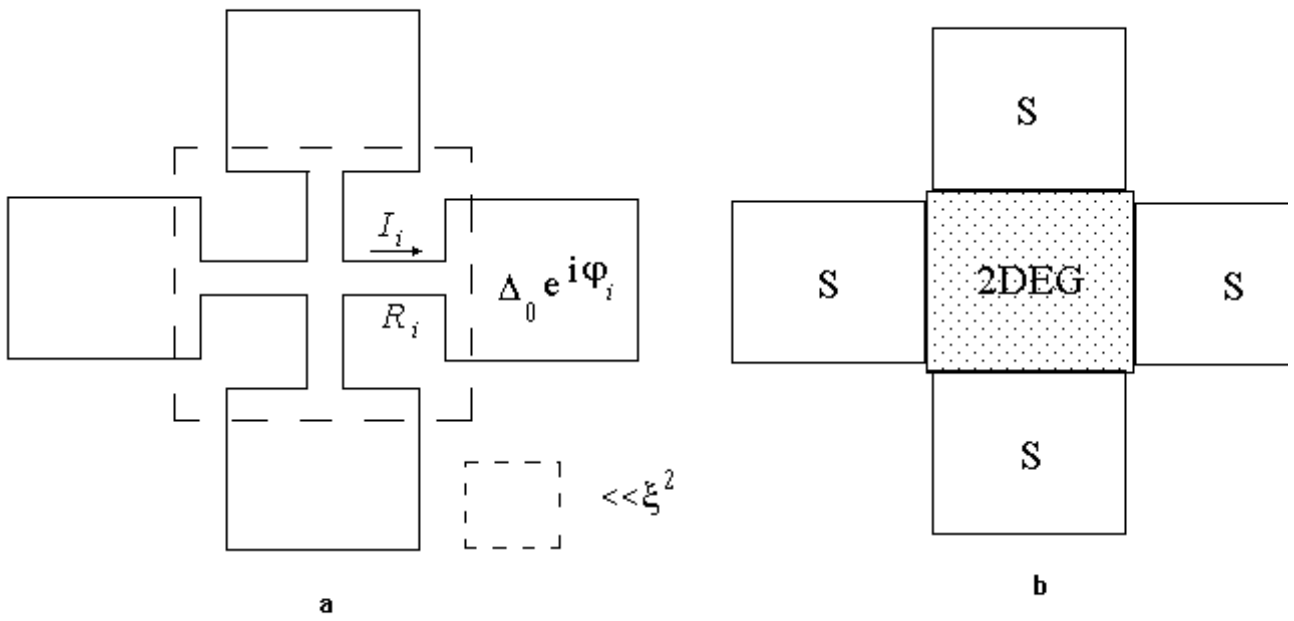


Figure 1

]

—

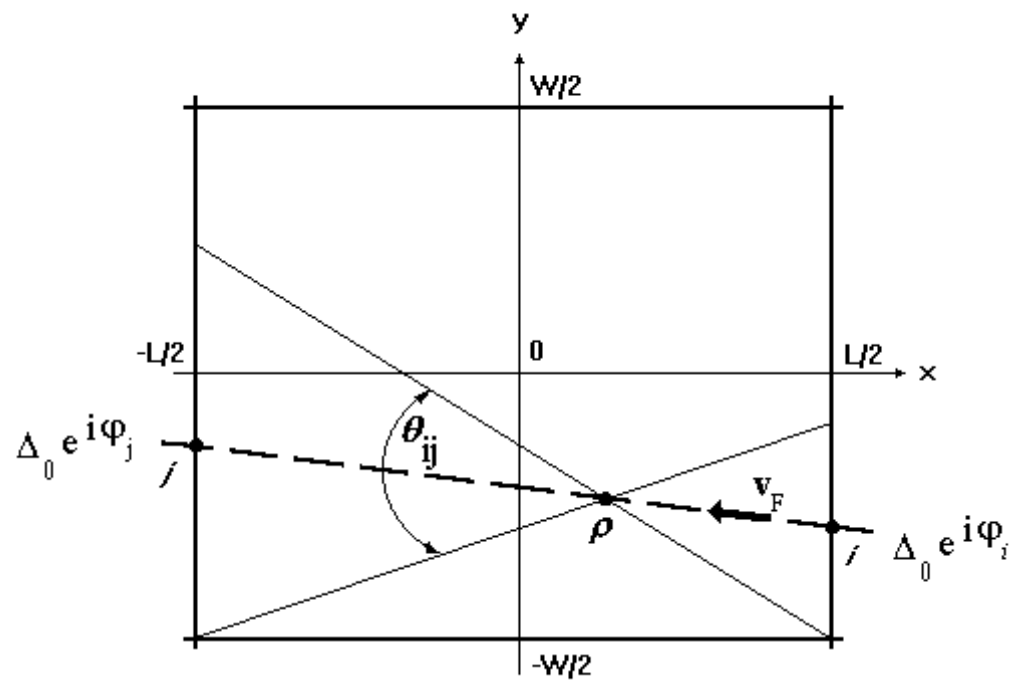


Figure 2

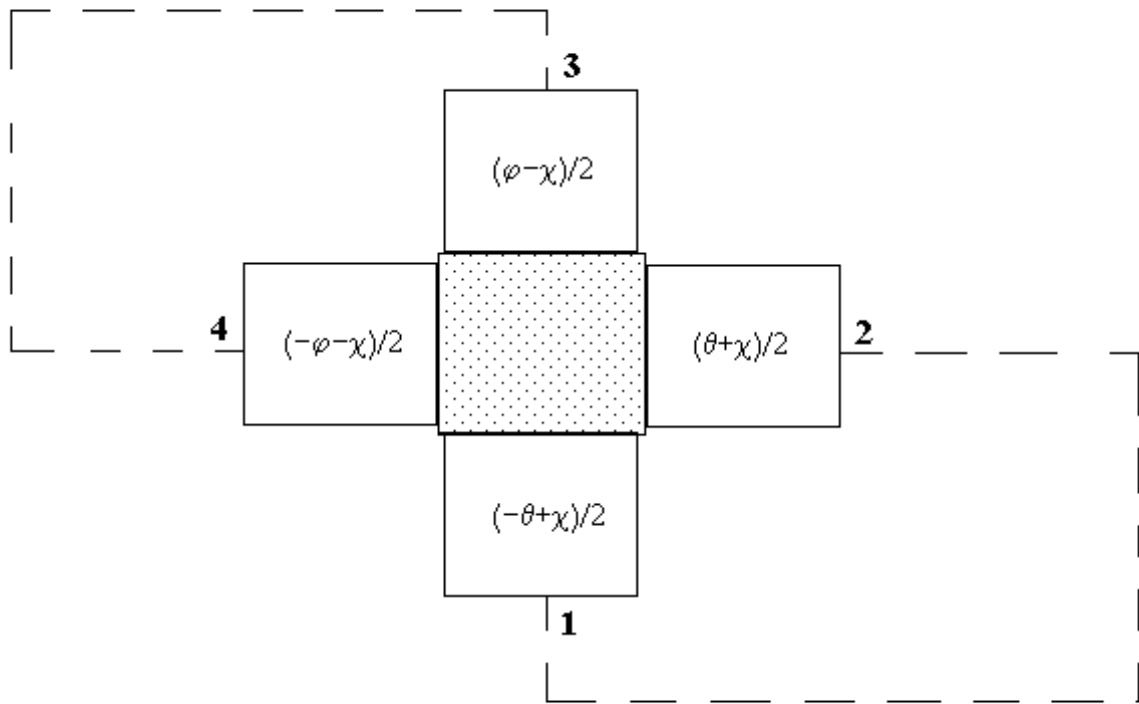
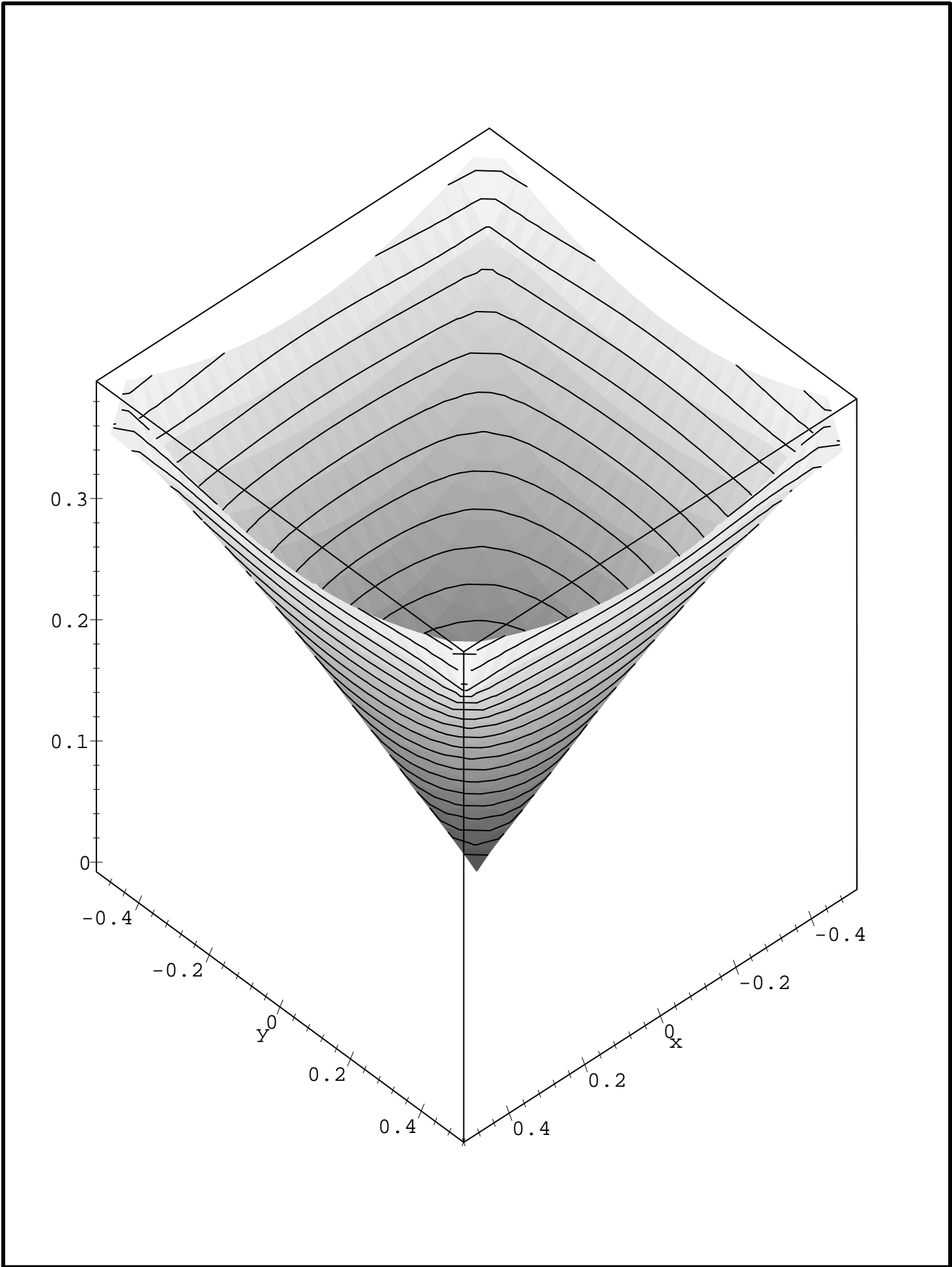
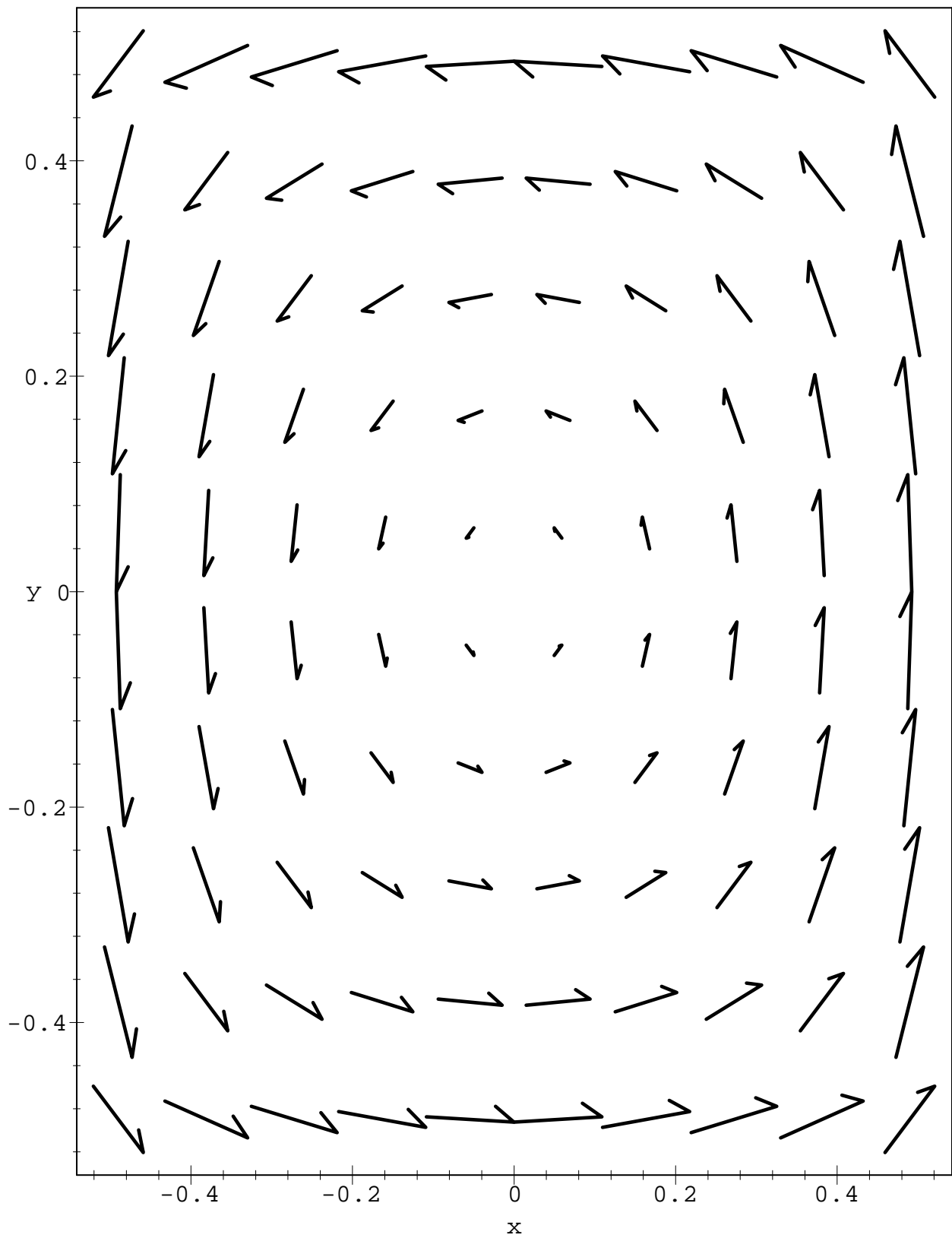


Figure 3





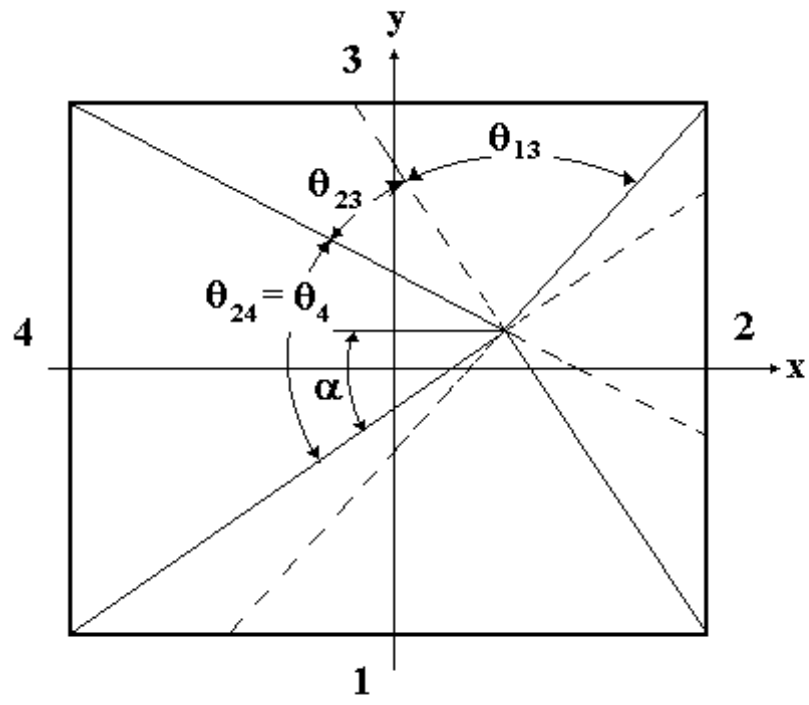


Figure 6
